Volume 1 | Number 1 | Jan 2013 | Pages 1–100

Journal of
Materials Chemistry B

Materials for biology and medicine
www.rsc.org/materialsB

ROYAL SOCIETY
OF CHEMISTRY

ROYAL SOCIETY
OF **CHEMISTRY**

www.rsc.org/materialsB

Journal Name

ARTICLE

Carborane-β-cyclodextrin complexes as supramolecular connector for bioactive surfaces

P. Neirynck,[a] J. Schimer,[b] P. Jonkheijm,[c] L.-G. Milroy,[a] P. Cigler,[b*] and L. Brunsveld[a*]

Supramolecular chemistry provides an attractive entry to generate dynamic and well-controlled bioactive surfaces. Novel host-guest systems are urgently needed to provide a broader affinity and applicability portfolio. A synthetic strategy to carborane-peptide bioconjugates was therefore developed to provide an entry to monovalent supramolecular functionalization of β-cyclodextrin coated surfaces. The β-cyclodextrin•carborane-cRGD surfaces are formed efficiently and with high affinity as demonstrated by IR-RAS, WCA, and QCM-D, compare favourable to existing bio-active host-guest surface assemblies, and display an efficient bioactivity, as illustrated by a strong functional effect of the supramolecular system on the cell adhesion and spreading properties. Cells seeded on the supramolecular surface displaying bioactive peptide epitopes exhibited a more elongated morphology, focal adhesions, and stronger cell adhesion compared to control surfaces. This highlights the macroscopic functionality of novel supramolecular immobilization strategy.

Introduction

Supramolecular host-guest chemistry has recently emerged as a versatile entry for the reversible immobilization of biomolecules on surfaces with retention of activity. For example, functional proteins and peptide epitopes modified with a ferrocene moiety have been immobilized on cucurbit[7]uril (CB7) surfaces with applications to protein arrays.[1–3] Similarly, beta-cyclodextrin (βCD) monolayers have been widely studied for the immobilization of ferrocene-labeled proteins or peptides via the ferrocene-βCD host-guest binding.[4,5] However, the relatively weak binding of βCD to ferrocene necessitates for multivalent interactions to enable efficient surface immobilization on βCD monolayers.[6,7] Rapid and efficient supramolecular protein and cell adhesion thus requires new guest molecules with alternative chemotypes and strong binding affinities to βCD-functionalized surfaces.

Carboranes are icosahedral cluster compounds consisting of boron, carbon and hydrogen atoms. Their exceptional chemical stability, caused by pseudo-aromatic delocalization of electrons, as well as their high resistance to biological degradation predisposes carboranes to various biomedical applications. Their high boron content renders carboranes useful for boron neutron capture therapy,[8] while their well-defined structure and distinctive hydrophobic properties makes them useful molecular scaffolds for drug development,[9,10] including as pharmacophores with tunable geometry and peripheral substitution for the construction of various tight-binding enzyme inhibitors such as carbonic anhydrase[11] and HIV protease.[12] Within the supramolecular field carboranes[13–17] and metallacarboranes[18–20] are highly appreciated due to their ability to form strong non-covalent complexes with cyclodextrins. For example, the host-guest interaction between βCD and carborane is used for chromatographic separations[21,22] and for the solubilization of carborane complexes containing platinum(II)-based DNA intercalators.[23,24]
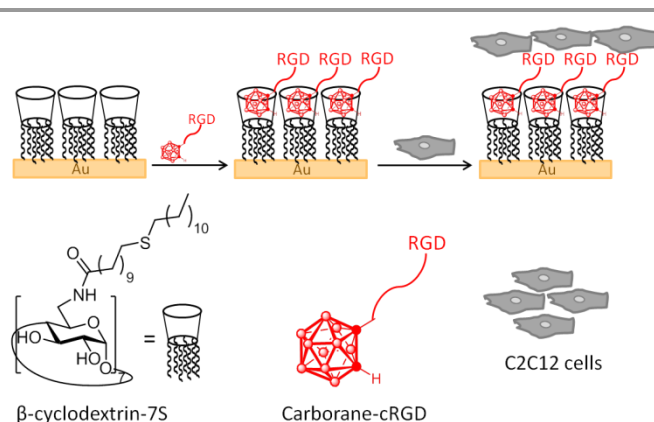

Figure 1. Bioactive surfaces via the supramolecular assembly of carborane-β-cyclodextrin complexes on gold or glass (not shown). A β-cyclodextrin monolayer is supramolecularly coated with a bioactive peptide sequence using the strong monovalent recognition of a carborane conjugated to the cyclic RGD motif. The functionality of the supramolecular platform is evidenced at the macroscopic level via the subsequent, substrate selective, recruitment, adhesion, and spreading of cells.

Here we use 1,2-closo-carborane (Cb) as a monovalent supramolecular guest molecule for the efficient non-covalent immobilization of biologically active peptides on βCD surfaces (Figure 1). We demonstrate the potential utility of the approach for the generation of biomaterials and cell adhesion applications by immobilizing integrin-binding peptides as a means to

selectively enhance adhesion and cell spreading of C2C12 cells to the supramolecular functionalized βCD monolayer.

Materials and methods

TBTU (O-(Benzotriazol-1-yl)-N,N,N′,N′-tetramethyluronium tetrafluoroborate) was supplied by Iris Biotech. The βCD derivatives were a kind gift from Dr. Alejandro Mendez Ardoy (University of Twente, The Netherlands). Amino acids were supplied by Novabiochem. Other chemicals and solvents were purchased from Sigma-Aldrich. Carboranes 1 to 3 were purified using column chromatography on silica (Sigma, pore size 60 Å, 70-230 mesh, 63-200 μm). The peptide conjugates were purified using preparative scale RP-HPLC Waters Delta 600 (flow rate 7 mL/min, gradient shown for each compound - including R_t) with column Waters SunFire C_{18} OBD Prep Column, 5 μm, 19 x 150 mm. Compound purity was determined by analytical Jasco PU-1580 HPLC (flow rate 1 mL/min, invariable gradient 2-100 % MeCN in 30 minutes, R_t shown beside each compound) with column Watrex C_{18} Analytical Column, 5 μm, 250 x 5 mm. Compounds were characterized using HRMS at LTQ Orbitrap XL (Thermo Fisher Scientific) and NMR (Bruker Avance I™ 400 MHz). Products 4 to 7 were purified using RP-HPLC on a Shimadzu HPLC equipped with surveyor PDA (C18 preparative column from Phenomenex (21.20 x 150 mm), flow rate 15 mL/min). Analysis was performed using LCQ Fleet from Thermo Scientific on a C18 column equipped with surveyor AS and PDA. Eluent conditions ($CH_3CN/H_2O/0.1\%$ HCO_2H) for 15 min run: 0-1 min, isocratic, 5 % CH_3CN; 1-10 min, linear gradient, 5 – 100 %; 10-11 min, isocratic, 100 %; 11-12 min, linear gradient, 100 - 5 %; 12-15 min, isocratic, 5 % CH_3CN, flow rate 0.1 mL/min.

Synthesis of carborane-cRGD and carborane-cRAD conjugates

Aminoethyl-o-carborane hydrochloride (1). 1.79 g (1.0 eq, 14.7 mmol) of decaborane (KatChem) was dissolved in 50 mL of dry toluene along with 2.75 g (1.0 eq, 14.7 mmol) of 2-(prop-2-yn-1-yl)isoindoline-1,3-dione. 1.286 g (0.5 eq, 7.36 mmol) of 1-butyl-3-methylimidazolium chloride was added and the reaction mixture refluxed overnight. The toluene was then evaporated and the organic slurry extracted 3x with Et_2O (50 mL). Organic phases were combined and evaporated to dryness. The product was further recrystallized from hot DCM to obtain pure product at 41 % yield (1.821 g, 8.72 mmol). The next two steps in synthesis were conducted as described previously and the data collected was identical to previously reported data.[25]

Carborane-cysteine (3). 530 mg (1.2 eq, 1.14 mmol) of Boc-Cys(Trt)-OH was weighed out in a round-bottom flask and dissolved in 3 mL of DMF. TBTU (367 mg, 1.2 eq, 1.14 mmol) and DIPEA (367 μL, 3.5 eq, 3.34 mmol) were then added and the reaction mixture left stirring for 15 min after which (aminoethyl)-o-carborane hydrochloride 1 (200 mg, 1.0 eq, 0.95 mmol) was added in one portion. All volatiles were evaporated after 12 h and the organic slurry dissolved in 20 mL of EtOAc. This solution was then washed 2x with a 10% solution of $KHSO_4$ (20 mL), 2x with a saturated solution of $NaHCO_3$ (20 mL) and once with brine. The organic layer was then dried and evaporated. The crude product was purified by column chromatography (hexane:EtOAc 5:1, R_f = 0.35; UV detection). 350 mg (0.57 mmol) of the protected product 2 was obtained in a 65% yield. The trityl- and boc- protecting groups were then cleaved off by treating 2 for 1 h with 1 mL of

TFA/H_2O/triisopropylsilane (95/2.5/2.5, %v/v). Purification by preparative scale HPLC (gradient 15-50 % MeCN in 40 minutes; R_t = 17 mins) afforded 65 mg of 3 as white powder upon lyophilization (42 % yield, purity > 95%). Note that the addition of acetone to 3 leads to stable thiazolid-2-one. Analytical HPLC R_t = 18.5 min. HRMS (ESI+): calculated for $C_6H_{21}ON_2SB_{10}$ [MH]$^+$ 279.22997. Found 279.23010. ^{1}H NMR (400 MHz, CD_3CN) δ 8.11 (bs, 1H), 4.33 (bs, 1H), 4.22 (t, J = 5.4 Hz, 2H), 3.98 (qd, J = 15.3, 6.7 Hz, 2H), 3.06 (ddd, J = 20.7, 14.9, 5.3 Hz, 2H), 2.85–1.35 (m, 12H). ^{13}C NMR (101 MHz, CD_3CN) δ 168.46 (s), 75.86 (s), 62.02 (s), 55.52 (s), 45.03 (s), 26.07 (s). ^{11}B NMR (128 MHz, CD_3CN, decoupled) δ -2.99 (s), -5.88 (s), -9.99 (s), -11.86 (s), -13.20 (s).

cRGD-maleimide 4 and cRAD-maleimide 5. cRGD and cRAD were synthesized according to previous literature.[2] 20 mg of peptide was reacted with NHS-activated maleimide (synthesized according to previous literature, see SI)[26] (1.4 eq.) in dry DMF (1 mL) for 1 h at rt in the presence of DIPEA (4 eq.). The solvents were then removed *in vacuo* and the peptide-maleimide conjugates were purified by preparative-RP HPLC (gradient 10 - 25% MeCN, 0.1 % HCO_2H in 20 min) to afford cRGD-maleimide 4 and cRAD-maleimide 5 in yields of 25% and 28%, respectively, both as white powders. 4: Analytical HPLC R_t = 2.55 min. MS (ESI+): calculated for $C_{34}H_{46}N_{10}O_{10}$ [MH]$^+$ 755.79 Found 755.67. 5: Analytical HPLC R_t = 2.55 min. MS (ESI+): calculated for $C_{35}H_{49}N_{10}O_{10}$ [MH]$^+$ 769.79 Found 769.67.

Cb-cRGD 6 and Cb-cRAD 7. 5.8 mg of cRGD-maleimide (resp. 3 mg of cRAD-maleimide) was dissolved in PBS (30 mM sodium phosphate, 50 mM NaCl, pH 7.4) and added to 1 (1 eq.) dissolved in 1 mL DMF. The reaction was stirred at room temperature for 1 h and the solvents were removed *in vacuo*. Purification was performed using preparative RP-HPLC (gradient 20-50% MeCN, 0.1 % HCO_2H in 30 min). Yields for Cb-cRGD 6 and Cb-cRAD 7 were 63 and 5 %, respectively. 6: Analytical HPLC R_t = 4.48 min. MS (ESI+): calculated for $C_{40}H_{67}B_{10}N_{12}O_{11}S$ [MH]$^+$ 1033.21. Found 1032.75. 7: Analytical HPLC R_t = 4.49 min. MS (ESI+): calculated for $C_{41}H_{70}B_{10}N_{12}O_{11}S$ [MH]$^+$ 1047.25. Found 1046.75.

Surface chemistry

βCD immobilization on glass coverslips. Glass coverslips were sonicated for 10 min in Hellmanex, then twice for 5 min in H_2O, dried under N_2 flow and exposed to O_2 plasma for 30 s. Surfaces were thoroughly washed with H_2O, then with EtOH and dried under N_2 flow. Surfaces were placed in a vacuum dessicator overnight with (trimethoxysilyl) propyl-ethylenediamine (TPEDA). The next day, the surfaces were washed with EtOH, dipped in dry toluene and then dried. Surfaces were incubated in a 1 mM toluene solution of 1,4-phenylene diisothiocyanate at 50 °C for 2 h under N_2 atmosphere, washed with toluene, EtOH and water, and subsequently incubated for 2 h at 50 °C with a 1 mM solution of per-6-amino-b-cyclodextrin (βCD-7NH$_2$, 8, Scheme 1) in H_2O.[27] Finally, the surfaces were washed sequentially with H_2O, EtOH and then thoroughly dried under N_2 flow.

Where applicable, substrates were then incubated for 3 h with 75 μL of a 100 μM aqueous solution of the carborane-peptide conjugate, rinsed with H_2O and dried under N_2 flow.

βCD immobilization on gold substrates. Prior to use in QCM-D experiments, resonators were activated for 15 s using a piranha solution (H_2SO_4/H_2O_2, 3:1, %v/v). Surfaces were then extensively washed with H_2O, EtOH, and then incubated in a 1 mM solution of heptakis{6-deoxy-6-[12-

(thiododecyl)undecanamido]}-β-cyclodextrin (βCD-7S, **9**, Scheme 1) for efficient immobilization[28,29] in CHCl$_3$/EtOH 2/1, heated at 60 °C for 1 h, then left at room temperature overnight, under a N$_2$ atmosphere. They were then rinsed with EtOH and dried under N$_2$ flow. The same protocol was followed for the preparation of substrates for IR-RAS analysis. Where applicable, the substrates were then incubated for 3 h with 75 µL of a 100 µM aqueous solution of the carborane-peptide conjugate, rinsed with H$_2$O and dried under N$_2$ flow.

Characterization of βCD – carborane-peptide surfaces. Fourier Transform Infrared Reflection Absorption Spectroscopy (FT-IR-RAS) measurements utilized 200 nm gold Si wafers, 2x2 cm. Polarized FT-IR-RAS spectra of 1000 scans with a resolution of 2 cm^{-1} were obtained using a Thermo Scientific TOM optical module.

Water contact angle measurements were performed on a Krüss G10 contact angle measuring instrument, equipped with a CCD camera. Images were analyzed using the Drop Shape Analysis software version 1.90.0.2 and ImageJ Contact Angle plug-in.

QCM-D studies. QCM-D data were measured using a Q-Sense E1 with a peristaltic pump, Ismatec Reglo Digital M2-2/12. Gold-coated QCM-D resonators QSX 301 with a resonance frequency of 4.95 MHz +/- 0.05 MHz were purchased from LOT-QuantumDesign. All solutions of Cb-cRGD were prepared using PBS buffer. Measurements were performed at 20 °C, with a flow of 50 µL/min. Prior to the binding of the Cb-RGD **6**, surfaces were equilibrated by flowing over PBS buffer until a stable baseline was obtained.

Cell culture and adhesion studies

C2C12 cells, from a mouse myoblast cell line, were used at passage between 15 and 20 for the cell experiments. 80% confluent T25 or T75 flasks of C2C12 were trypsinized, centrifuged and redispersed in DMEM medium supplemented with penicillin/strep, NEAA, as well as 10% FBS for culturing and 0% FBS for surface incubation experiments.

Glass substrates coated with βCD and carborane-peptide were dipped in and out into 70% EtOH and rinsed twice with PBS. Cells in suspension in 0% FBS supplemented DMEM media were seeded on the substrates (20 000 cells/mL, 3 mL/well) and left to adhere for 1 h at 37 °C and 5% CO$_2$. Surfaces were then gently washed twice with PBS, cells were fixed for 10 min with 10% formalin and then rinsed three times with PBS.

Cells were incubated with blocking solution (0.1% Triton, 0.5% w/w BSA in PBS pH 7.4) for 1 h at room temperature or overnight at 4 °C. Surfaces were then incubated with Paxillin 1:500 in blocking buffer for 1 h, washed 3 times for 10 min with blocking buffer, and incubated for 1 h with secondary antibody-Alexa 488 (1:500) and phalloidin-Alexa 546 (1:500) in blocking buffer. Finally the surfaces were washed once for 10 min with blocking buffer and twice with PBS, incubated for 10 min with DAPI in PBS (1:1000), rinsed with PBS three times, and then stored at 4 °C.

Imaging was performed using an Olympus IX71 fluorescence microscope, at 40x magnification. Five pictures per substrate were taken for each of the three repetitions and analysis of the cell adhesion was performed using CellProfiler.[30] Cells that could not be recognized by the software or that did not fall completely in the field of view were discarded from the analysis. On average, between 30 and 40 cells per substrate per set remained for analysis, corresponding to approximately 100 cells per condition. Results were normalized towards the average value obtained for each experiment set for the βCD control surface. All experiments were performed in triplicate.

Results and discussion

Synthesis

Our aim was to develop conditions to couple the carborane to biomolecules, which might be compatible with a broad range of molecules including peptides and proteins. Therefore thiol-functionalized carboranes[31,32,33,34] were explored to react with maleimide modified peptides under mild conditions. Direct connection of the thiol to the Cb cage,[31,32] is expected to lead to steric hindrance regarding βCD binding and peptide conjugation. A water-soluble Cb bearing a thiol group attached via a short linker,[33,34] would constitute a more beneficial starting point. Therefore, the 1-aminomethyl-1,2-*closo*-carborane precursor was first prepared in three steps starting from decaborane B$_{10}$H$_{14}$ (see Scheme 1). We modified the previously published synthesis[25] by implementing a recently described acetylene insertion methodology, which is performed in ionic liquid.[35] The aminomethyl-carborane **1** was then coupled to the protected cysteine Boc-Cys(Trt)-OH via TBTU activation and the desired product, **3**, obtained upon treatment with TFA/H$_2$O/triisopropylsilane (95/2.5/2.5, %v/v) without evidence of thiol capping. Peptide activation was performed at pH 7 to favor selective coupling of the NHS-activated maleimide to the lysine, providing **4** and **5**. Reactions between the Cys-functionalized Cb and the maleimide-cRGD and maleimide-cRAD were performed in a 1:1 (v/v) mixture of DMF/PBS at pH 7-7.5 to afford the target compounds **6** and **7**.
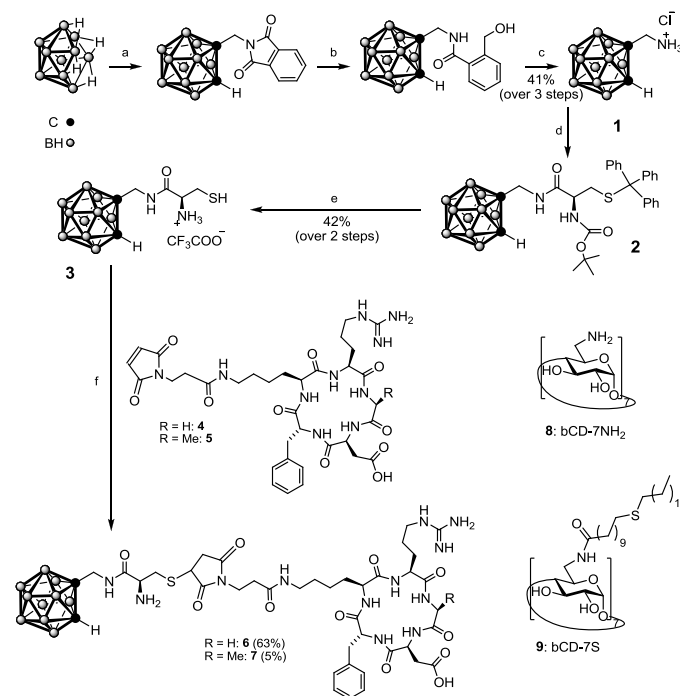
Scheme 1. Structures of βCD-7NH$_2$ **8**[27] and βCD-7S **9**[28,29] and synthesis of carborane-thiol **3** and peptide-carborane conjugates, **6** (cRGD) and **7** (cRAD). a) 2-(prop-2-yn-1-yl)isoindoline-1,3-dione, [BMIM]Cl, toluene, 110 °C; b) NaBH$_4$, *i*-PrOH/H$_2$O; c) AcOH/H$_2$O, HCl, 75 °C; d) Boc-Cys(Trt)-OH, TBTU, DIPEA, DMF; e) TFA/H$_2$O/TIS; f) DMF/PBS 1/1 %(v/v), 1 h, rt. BMIM = 1-Butyl-3-methylimidazolium, TBTU = O-(Benzotriazol-1-yl)-N,N,N',N'-tetramethyluronium tetrafluoroborate, DIPEA = N,N-diisopropylethylamine, DMF = N,N-dimethylformamide, TIS = triisopropylsilane.

Surface characterization

Water contact angle (WCA) measurements were performed to provide information on changes in the hydrophilicity of the surface upon successive monolayer formation (Figure 2). A large decrease in contact angle was observed – from 95 to 49 degrees – after functionalization of gold surface with βCD-7S, which display several OH groups and thus increase the hydrophilicity of the surface. Subsequent incubation with Cb-cRGD, **6**, resulted in an an small increase in WCA of the polar surface from 49 to 56 degrees, in agreement with previously reported values for RGD functionalized surfaces.[2]

Figure 2. Water contact angle values for gold, βCD monolayer and βCD complexed with Cb-cRGD **6** (n=4), with a representative picture. A high WCA angle value indicates a hydrophobic surface.
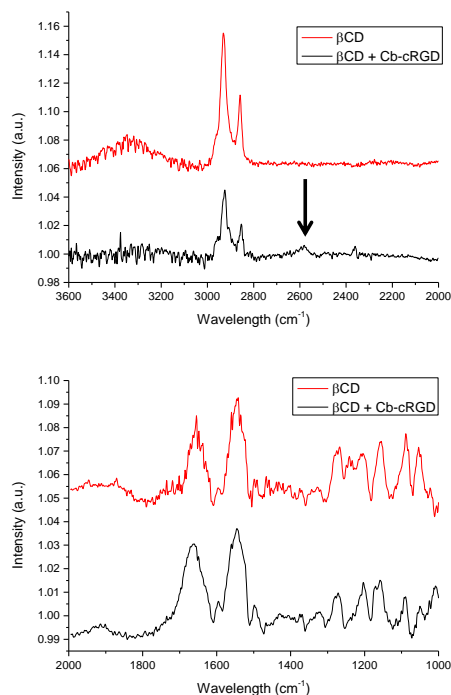

Figure 3. FT-IR-RAS of βCD (red) and βCD + Cb-cRGD, **6** (black) on gold, in two different regions (top: 3600 – 2000 cm^{-1}, bottom: 2000 - 1000 cm^{-1}). The arrow shows a characteristic peak of a βCD•carborane complex.

To get more insight into the formation of the βCD•Cb complex on gold, substrates functionalized with bCD-7S[28,29] and further incubated with Cb-cRGD **6** were studied by Infrared Reflection Absorption Spectroscopy (IR-RAS). The IR spectrum of βCD[36] in solution exhibits characteristic absorption peaks at 1053, 1088, 1157, 1204, 1241 and 1267 cm^{-1} – corresponding to different stretching (CO and CC), and bending modes (COH, OCH and CCH), which are also observed on the gold surface (Figure 3). Sharp peaks at 1654 cm^{-1} (βCD) and 1661 cm^{-1} (βCD + Cb-cRGD) were observed corresponding to the C=O

stretch of amides present in βCD-7S structure as well as in the cRGD peptide conjugates, while the intense broad peak at 3345 cm^{-1} is characteristic of the presence of secondary OH groups. A peak at 2582 cm^{-1} (B-H) (Figure 3 top, arrow) is observed in the case of βCD + Cb-cRGD, which is indicative of complexation between βCD and Cb and has also been observed for a similar system in solution.[37,38] Both surface analyses provide convincing evidence for the immobilization of carborane-peptide conjugates to the βCD-7S gold monolayers via the βCD•carborane complexation.

Host-guest surface complexation

Quartz Crystal Microbalance with Dissipation monitoring (QCM-D) measurements were performed for a more detailed and quantitative analysis of the affinity of Cb-cRGD (**6**) for βCD monolayers. In general, a change at the surface of a quartz crystal sensor, for example via binding of a compound, results in a measurable change in the vibration frequency of the sensor. Various concentrations of Cb-cRGD (**6**) in PBS, ranging from 10 to 500 μM, were flown over gold crystals pre-functionalized with βCD-7S (Figure 4a). Dissipation remained within 10% of the change in frequency value, indicating the formation of a rigid film at the resonator surface and allows the Sauerbrey model to be applied.[39] The change in frequency of the 5th resonance was plotted versus the concentration of **6** (Figure 4b) and the resulting graph could be fitted with a Langmuir model, providing a K_d value of 178 μM +/- 39 μM for the interaction of **6** for the βCD monolayer, via the Cb mediated host-guest interaction.
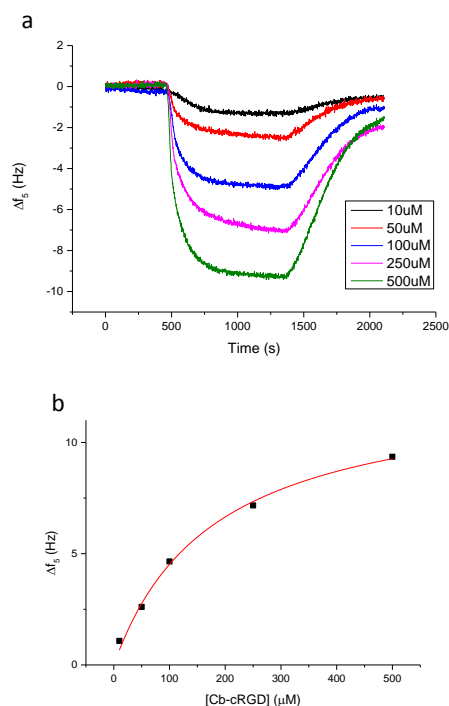

Figure 4. QCM-D data forbinding of Cb-cRGD (**6**) to βCD-7S coated quartz crystals. a) Fifth resonance frequency overtone (Δf_5) for various concentrations of Cb-cRGD (10, 50, 100, 250, 500 uM). b) Change in frequency of the fifth overtone versus Cb-cRGD concentration. Fit was performed using Origin, Langmuir fit, resulting in a K_d value of 178 μM +/- 39 μM.

The affinity of carborane **6** for the βCD monolayer compares favorably with other known guests of βCD, such as ferrocene and adamantane. Carborane binds to βCD with 5-fold greater affinity than aminomethylferrocene derivatives and is therefore better suited for monovalent surface immobilization.[4] Lithocholic acid binds to βCD with high binding affinity in solution ($K_d = 1.2*10^{-6}$ M), but has limited potential for βCD surface interactions due to the guest protruding the βCD at the smaller ring, resulting in lowered affinities.[40] The affinities of carborane and adamantane for a βCD monolayer are comparable.[41] However, carborane introduces to the system a unique quality: high content of boron, which in principle can be further utilized for quantification of conjugation yields using sensitive spectral method such as inductively atomic emission spectrometry with inductively coupled plasma (ICP AES), as has been shown for boron-containing BODIPY dyes.[42]

Cellular evaluation of the surfaces

Strong and directional supramolecular surface immobilization strategies provide substantial opportunities for biomedical applications. To explore the potential of the βCD-Cb complex in this respect, the ability of surface-immobilized Cb-cRGD conjugates to induce specific cell adhesion was studied using the C2C12 mouse myoblast cell line. C2C12 cells express various integrin receptors, including $\alpha_v\beta_3$, which is known to bind to cRGDfK, as used in **6**,[43,44] and show clear phenotypic changes to the environment.[45,46] For these experiments, cells were passaged at 80% confluence to avoid differentiation. While the surface characterization was performed on gold surfaces coated with βCD (*vide supra*), glass surfaces are more suitable for fluorescence microscopy studies and were thus favored for the cell experiments. Surfaces featuring a βCD monolayer and a βCD monolayer complexed with bio-inactive conjugate Cb-cRAD **7** were used as reference surfaces. Cyclodextrins are composed of oligomerized glucose and therefore do not specifically discourage cell adhesion, but lack a specific molecular entity to enhance cell spreading, such as the bioactive epitope cRGD. Cells seeded on either the control βCD or βCD + Cb-cRAD substrates remained round and did not form proper focal adhesions (Figure 5a,b). However, cells seeded on the βCD + Cb-cRGD surfaces became strongly anchored to the surface, evident already within 1 h of seeding, with pronounced stretching of actin filaments as a consequence of cell and focal adhesion (Figure 5c). These results show that the cells specifically recognize the RGD sequence through binding to integrins, and that the differences in cell morphology observed between the βCD + Cb-cRGD and βCD + Cb-cRAD surfaces are a specific consequence of the difference in integrin binding affinities between the supramolecular immobilized cRGD and cRAD.[47]
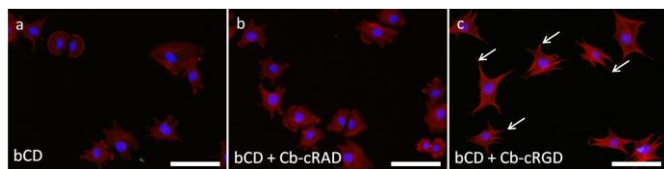

Figure 5. Scale bar: 50 μm. C2C12 seeded on glass surfaces coated with a) βCD, b) βCD and Cb-cRAD, c) βCD and Cb-cRGD, fixed after 1 h and stained for nucleus (DAPI) and actin (Phalloidin). Focal adhesions are exemplary indicated by the white arrows.

A more in-depth analysis of the cell adhesion was performed using CellProfiler[30] to obtain a quantitative difference in cellular morphological properties under the different surface immobilization conditions (Figure 6). Similar studies have been performed to correlate qualitative and quantitative aspects of cell pictures.[48,49] A workflow chart providing information about e.g. cell area, perimeter or eccentricity was run and data were analyzed using the software GraphPad Prism. A repeated-measures one-way analysis of variance (one-way ANOVA) test was applied on the normalized averages for each repetition and each condition. As already indicated by the simple visual aspect and observation of the focal adhesions, statistically noticeable differences in eccentricity, perimeter, form factor, compactness and ratio between the major and minor axis lengths was only observed for the βCD monolayer complexed with Cb-cRGD compared to βCD; there is a significant difference ($p < 0.05$) between the control surface βCD and the active surface (βCD with Cb-cRGD).
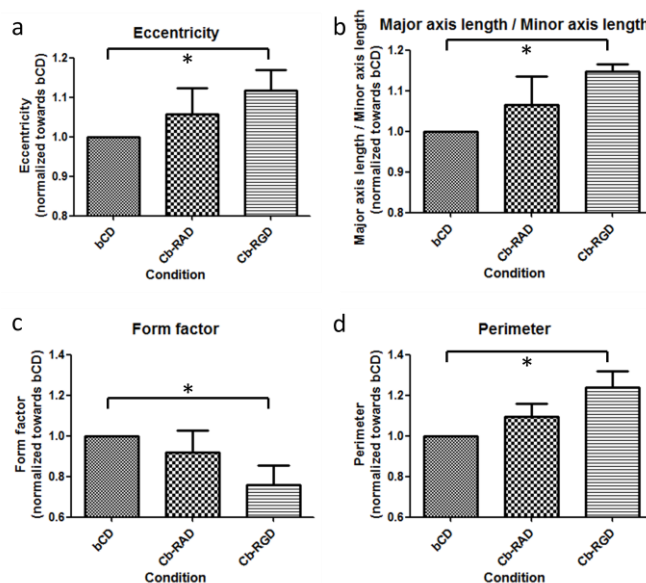

Figure 6. Statistical analysis of the cell experiments with CellProfiler[30] and GraphPad Prism. Data were normalized and averaged for each repetition towards the control βCD.

Some of the morphological characteristic changes strongly correlate with one another. For example, the eccentricity describes the elliptical character of the cell morphology (Figure 6a): an increase in eccentricity describes a shape that transitions from a circle, through an ellipse, to a line. In line with this, the ratio of the major axis length divided by the minor axis length will be higher in the case of an elongated cell compared to a cell displaying a more rounded morphology (Figure 6b). These observations can specifically be made for the supramolecular adhered cells; the eccentricity increases from 1 for βCD to 1.12 for the Cb-cRGD surface. The ratio of the axis lengths also increases, from 1 to 1.14. The form factor is defined as $4\pi*area/perimeter^2$: this value will be equal to 1 for a circle and will decrease as the perimeter of the cell increases (Figure 6c). An increase in the perimeter (from 1 to 1.24) (Figure 6d) can be observed which correlates with a decrease in the form factor (1 to 0.76). These results confirm the qualitative observation from the pictures and thus the functional effect of the supramolecular system on the cell adhesion and spreading properties: cells are

more elongated and functionally adhered on the βCD + Cb-cRGD surface than on the control surfaces.

Conclusions

Supramolecular systems offer great opportunities for the development of dynamic and well-controlled biocompatible surfaces and coatings. Existing host-guest elements require optimization regarding affinity and applicability. Here, we reported the synthesis of a carborane derivative mono-functionalized with cysteine for conjugation to biologically relevant molecules, such as peptides, under mild conditions. The utility of the approach was demonstrated by conjugating the cysteine-carborane derivative to cRGD analogs via Michael 1,4-addition to a maleimide group under ambient conditions (room temperature, pH 7-7.5). Though not demonstrated here, the functionalization of whole proteins with the cysteine-carborane derivative via expressed protein ligation or maleimide coupling should also be possible. Formation of the βCD•carborane-cRGD complex on surfaces was demonstrated by IR-RAS and WCA, and the binding affinity quantified by QCM-D, comparing favorable to existing bio-active host-guest assemblies on βCD surfaces. Cells seeded on βCD + Cb-cRGD substrates exhibited a more elongated morphology and stronger cell adhesion compared to control βCD and βCD + Cb-cRAD substrates, showing the functionality of the supramolecular immobilization strategy on the macroscopic level. This opens new possibilities to generate innovative and robust supramolecular surfaces of biomedical interest.

Acknowledgements

Notes and references

[a] Laboratory of Chemical Biology and Institute of Complex Molecular Systems (ICMS), Department of Biomedical Engineering, Eindhoven University of Technology, Den Dolech 2, 5612 AZ, Eindhoven, The Netherlands Fax: (+31) 40-247-8367; E-mail: l.brunsveld@tue.nl
[b] Institute of Organic Chemistry and Biochemistry AS CR, v.v.i., Flemingovo nam. 2, Prague 6, 166 10, Czech Republic, Tel.: +420-220-183-429, Fax: +420-224-310-090, E-mail: cigler@uochb.cas.cz
[c] Molecular Nanofabrication Group, MESA+ Institute for Nanotechnology, Department of Science and Technology, University of Twente, P.O. Box 217, 7500 AE, Enschede, The Netherlands; E-mail: p.jonkheijm@utwente.nl
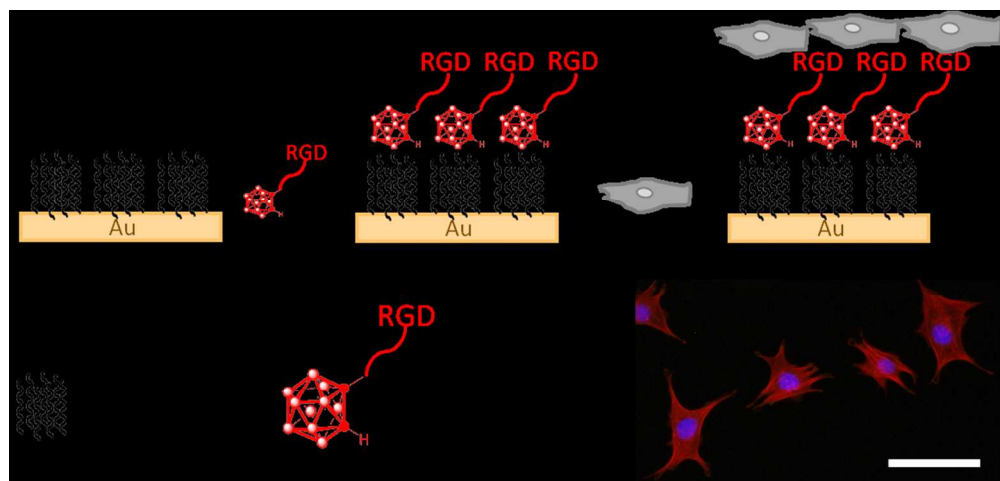
1. J. F. Young, H. D. Nguyen, L. Yang, J. Huskens, P. Jonkheijm, and L. Brunsveld, *ChemBioChem*, 2010, **11**, 180–183.
2. P. Neirynck, J. Brinkmann, Q. An, D. W. J. van der Schaft, L.-G. Milroy, P. Jonkheijm, and L. Brunsveld, *Chem. Commun.*, 2013, **49**, 3679–3681.
3. I. Hwang, K. Baek, M. Jung, Y. Kim, K. M. Park, D.-W. Lee, N. Selvapalam, and K. Kim, *J. Am. Chem. Soc.*, 2007, **129**, 4170–4171.
4. L. Yang, A. Gomez-Casado, J. F. Young, H. D. Nguyen, J. Cabanas-Danés, J. Huskens, L. Brunsveld, and P. Jonkheijm, *J. Am. Chem. Soc.*, 2012, **134**, 19199–19206.
5. D. Thakar, L. Coche-Guérente, M. Claron, C. H. F. Wenk, J. Dejeu, P. Dumy, P. Labbé, and D. Boturyn, *ChemBioChem*, 2014, **15**, 377–381.
6. J. Guo, C. Yuan, M. Guo, L. Wang, and F. Yan, *Chem. Sci.*, 2014, **5**, 3261–3266.
7. M. Ortiz, M. Torréns, A. Fragoso, and C. K. O'Sullivan, *Anal. Bioanal. Chem.*, 2012, **403**, 195–202.
8. R. F. Barth, J. A. Coderre, M. G. H. Vicente, and T. E. Blue, *Clin. Cancer Res.*, 2005, **11**, 3987–4002.
9. F. Issa, M. Kassiou, and L. M. Rendina, *Chem. Rev.*, 2011, **111**, 5701–5722.
10. M. Scholz and E. Hey-Hawkins, *Chem. Rev.*, 2011, **111**, 7035–7062.
11. J. Brynda, P. Mader, V. Šícha, M. Fábry, K. Poncová, M. Bakardiev, B. Grüner, P. Cígler, and P. Řezáčová, *Angew. Chem.*, 2013, **125**, 14005–14008.
12. P. Cígler, M. Kožíšek, P. Řezáčová, J. Brynda, Z. Otwinowski, J. Pokorná, J. Plešek, B. Grüner, L. Dolečková-Marešová, M. Máša, J. Sedláček, J. Bodem, H.-G. Kräusslich, V. Král, and J. Konvalinka, *Proc. Natl. Acc. Sci.*, 2005, **102**, 15394–15399.
13. A. Harada and S. Takahashi, *Chem. Commun.*, 1988, 1352–1353.
14. C. Frixa, M. Scobie, S. J. Black, A. S. Thompson, and M. D. Threadgill, *Chem. Commun.*, 2002, 2876–2877.
15. K. Ohta, S. Konno, and Y. Endo, *Tet. Lett.*, 2008, **49**, 6525–6528.
16. R. Vaitkus and S. Sjöberg, *J. Incl. Phen. Macroc. Chem.*, 2011, **69**, 393–395.
17. H. Y. V. Ching, S. Clifford, M. Bhadbhade, R. J. Clarke, and L. M. Rendina, *Chem. Eur. J.*, 2012, **18**, 14413–14425.
18. P. A. Chetcuti, P. Moser, and G. Rihs, *Organometal.*, 1991, **10**, 2895–2897.
19. J. Rak, M. Jakubek, R. Kaplánek, P. Matějíček, and V. Král, *Eur. J. Med. Chem.*, 2011, **46**, 1140–1146.
20. M. Uchman, P. Jurkiewicz, P. Cígler, B. Grüner, M. Hof, K. Procházka, and P. Matějíček, *Langmuir*, 2010, **26**, 6268–6275.
21. H. Horáková, B. Grüner, and R. Vespalec, *Chirality*, 2011, **23**, 307–319.
22. P. Matějíček, M. Uchman, M. Lepšík, J. Srnec, J. Zedník, P. Kozlík, and K. Kalíková, *ChemPlusChem*, 2013, **78**, 528–535.
23. H. Y. V. Ching, D. P. Buck, M. Bhadbhade, J. G. Collins, and L. M. Rendina, *Chem. Commun.*, 2012, **48**, 880.
24. H. Y. V. Ching, R. J. Clarke, and L. M. Rendina, *Inorg. Chem.*, 2013, **52**, 10356–10367.
25. J. G. Wilson, A. K. M. Anisuzzaman, F. Alam, and A. H. Soloway, *Inorg. Chem.*, 1992, **31**, 1955–1958.
26. H. Y. Song, M. H. Ngai, Z. Y. Song, P. A. MacAry, J. Hobley, and M. J. Lear, *Org. Biomol. Chem.*, 2009, **7**, 3400–3406.
27. P. R. Ashton, R. Königer, J. F. Stoddart, D. Alker, and V. D. Harding, *J. Org. Chem.*, 1996, **61**, 903–908.
28. M. W. J. Beulen, J. Bügler, M. R. de Jong, B. Lammerink, J. Huskens, H. Schönherr, G. J. Vancso, B. A. Boukamp, H. Wieder, A. Offenhäuser, W. Knoll, F. C. J. M. van Veggel, and D. N. Reinhoudt, *Chem. Eur. J.*, 2000, **6**, 1176–1183.
29. M. W. J. Beulen, J. Bügler, B. Lammerink, F. A. J. Geurts, E. M. E. F. Biemond, K. G. C. van Leerdam, F. C. J. M. van Veggel, J. F. J. Engbersen, and D. N. Reinhoudt, *Langmuir*, 1998, **14**, 6424–6429.
30. A. E. Carpenter, T. R. Jones, M. R. Lamprecht, C. Clarke, I. H. Kang, O. Friman, D. A. Guertin, J. H. Chang, R. A. Lindquist, J. Moffat, P. Golland, and D. M. Sabatini, *Gen. Biol.*, 2006, **7**, R100.
31. J. Plešek and S. Heřmánek, *Coll. Czech. Chem. Commun.*, 1981, **46**, 687–692.
32. L. I. Zakharkin and G. G. Zhigareva, *Russ. Chem. Bull.*, 1967, **16**, 1308–1310.
33. J. A. Todd, P. Turner, E. J. Ziolkowski, and L. M. Rendina, *Inorg. Chem.*, 2005, **44**, 6401–6408.
34. D. Pietrangeli, A. Rosa, A. Pepe, and G. Ricciardi, *Inorg. Chem.*, 2011, **50**, 4680–4682.
35. Y. Li, P. J. Carroll, and L. G. Sneddon, *Inorg. Chem.*, 2008, **47**, 9193–9202.
36. O. Egyed, *Vibr. Spectros.*, 1990, **1**, 225–227.
37. A. Harada and S. Takahashi, *Chem. Commun.*, 1988, 1352–1353.
38. T. J. Tague and L. Andrews, *J. Am. Chem. Soc.*, 1994, **116**, 4970–4976.
39. G. Sauerbrey, *Z. Physik*, 1959, **155**, 206–222.
40. Z. Yang and R. Breslow, *Tet. Lett.*, 1997, **38**, 6171–6172.

41. D. A. Uhlenheuer, D. Wasserberg, C. Haase, H. D. Nguyen, J. H. Schenkel, J. Huskens, B. J. Ravoo, P. Jonkheijm, and L. Brunsveld, *Chem. Eur. J.*, 2012, **18**, 6788–6794.

42. P. Cigler, A. K. R. Lytton-Jean, D. G. Anderson, M. G. Finn, and S. Y. Park, *Nat. Mater.*, 2010, **9**, 918–922.

43. U. Hersel, C. Dahmen, and H. Kessler, *Biomaterials*, 2003, **24**, 4385–4415.

44. K.-E. Gottschalk and H. Kessler, *Angew. Chem. Int. Ed.,* 2002, **41**, 3767–3774.

45. S. Weis, T. T. Lee, A. del Campo, and A. J. García, *Acta Biomater.*, 2013, **9**, 8059–8066.

46. P.-Y. Wang, T.-H. Wu, W.-B. Tsai, W.-H. Kuo, and M.-J. Wang, *Colloids Surf. B: Biointerf.*, 2013, **110**, 88–95.

47. G. J. Strijkers, E. Kluza, G. A. F. V. Tilborg, D. W. J. van der Schaft, A. W. Griffioen, W. J. M. Mulder, and K. Nicolay, *Angiogenesis*, 2010, **13**, 161–173.

48. J. Boekhoven, C. M. Rubert Pérez, S. Sur, A. Worthy, and S. I. Stupp, *Angew. Chem. Int. Ed.*, 2013, **52**, 12077–12080.

49. J. E. Gautrot, J. Malmström, M. Sundh, C. Margadant, A. Sonnenberg, and D. S. Sutherland, *Nano Lett.*, 2014, **14**, 3945–3952.

The supramolecular carborane-β-cyclodextrin system allows for effective monovalent immobilization of biologically active peptides resulting in efficient cell adhesion and spreading.

196x93mm (150 x 150 DPI)